


Allosteric auto-inhibition and activation of the Nedd4 family E3 ligase Itch

Kang Zhu^{1,†}, Zelin Shan^{1,†}, Xing Chen^{1,†}, Yuqun Cai², Lei Cui³, Weiyi Yao¹, Zhen Wang¹, Pan Shi⁴, Changlin Tian⁴, Jizhong Lou³, Yunli Xie² & Wenyu Wen^{1,*} 

Abstract

The Nedd4 family E3 ligases are key regulators of cell growth and proliferation and are often misregulated in human cancers and other diseases. The ligase activities of Nedd4 E3s are tightly controlled via auto-inhibition. However, the molecular mechanism underlying Nedd4 E3 auto-inhibition and activation is poorly understood. Here, we show that the WW domains preceding the catalytic HECT domain play an inhibitory role by binding directly to HECT in the Nedd4 E3 family member Itch. Our structural and biochemical analyses of Itch reveal that the WW2 domain and a following linker allosterically lock HECT in an inactive state inhibiting E2-E3 transthiolation. Binding of the Ndfip1 adaptor or JNK1-mediated phosphorylation relieves the auto-inhibition of Itch in a WW2-dependent manner. Aberrant activation of Itch leads to migration defects of cortical neurons during development. Our study provides a new mechanism governing the regulation of Itch.

Keywords allosteric regulation; crystal structure; Itch; Ndfip1; Nedd4 family E3 ligases

Subject Categories Post-translational Modifications, Proteolysis & Proteomics; Structural Biology

DOI 10.15252/embr.201744454 | Received 8 May 2017 | Revised 7 July 2017 | Accepted 7 July 2017 | Published online 26 July 2017

EMBO Reports (2017) 18: 1618–1630

Introduction

Protein ubiquitination mediated by highly ordered E1-E2-E3 multi-enzyme cascades controls the cellular fates of a myriad of proteins through regulating proteins degradation, endocytosis, and trafficking of transmembrane proteins [1]. As the substrate specificity of ubiquitination is mainly governed by E3 ligases, E3s need to be tightly regulated and have attracted high attention as targets for therapeutic interventions [2–4]. The Nedd4 (neuronal precursor cell-expressed developmentally downregulated 4) family is the largest and best-characterized subgroup of HECT (homologous with

E6-associated protein C-terminus) type E3 ligases, comprising nine distinct members in mammals with unique functions (Appendix Fig S1A). Malfunctions of the Nedd4 E3s have been frequently identified in human cancers and other diseases [5–7]. Nedd4 member Itch plays a key role in the regulation of the immune responses of both mouse and human, including T-cell activation and tolerance and T-helper cell differentiation [8–13]. T-cell activation leads to JNK1-mediated phosphorylation and activation of Itch, resulting in Itch-dependent ubiquitylation and degradation of JunB, which regulates the transcription of the interleukin 4 (IL4) gene [14]. Besides, Itch couples JNK1 activation to tumor necrosis factor- α (TNF- α)-induced cell death by inducing proteasomal elimination of FLIP, an inhibitor of caspase 8-mediated apoptosis that is normally stimulated by NF- κ B [15]. Other substrates for Itch include Notch and the p53 relatives p63 and p73 [16–19].

The Nedd4 family displays a shared architecture comprising an N-terminal calcium/phospholipid-binding C2 domain for membrane localization, 2–4 central WW domains recognizing PY (PPxY) motifs in substrate proteins, and the C-terminal HECT domain which catalyzes the attachment of ubiquitin (Ub) to substrates (Appendix Fig S1A) [20]. HECT has a bilobal domain structure where the E2-binding N-lobe is connected by a flexible hinge loop to the C-lobe bearing the catalytic Cys residue. The known apo- or E2-bound HECT structures (including E6AP, WWP1, Smurf2, Nedd4, Nedd4L, and Itch) revealed that N- and C-lobes can adopt either an inactive T-shaped or a catalytically active L-shaped conformation [21–26]. In the E2-bound state, the flexible hinge region enables a conformational rearrangement, allowing the N- and C-lobes to come close together to juxtapose the E2 and E3 thiol groups for Ub transfer [25]. Mutations in the hinge region that restrict the conformational freedom inhibit the ubiquitination of WWP1, indicating that the structural plasticity of HECT E3 is required for catalytic activity [21]. In spite of the distinct organization, the isolated HECT domains from the Nedd4 family proteins show high ligase activity analyzed by *in vitro* auto-ubiquitination assay, though it was recently proposed that ubiquitylation-dependent oligomerization of HECT regulates the activity of Nedd4 ligases [27].

1 Department of Neurosurgery, Huashan Hospital, Institutes of Biomedical Sciences, Fudan University, Shanghai, China

2 Institutes of Brain Science, State Key Laboratory of Medical Neurobiology and Collaborative Innovation Center for Brain Science, Fudan University, Shanghai, China

3 Key Laboratory of RNA Biology, Institute of Biophysics, Chinese Academy of Sciences, Beijing, China

4 School of Life Sciences, University of Science and Technology of China, Hefei, China

*Corresponding author. Tel: +86 21 54237501; E-mail: wywen@fudan.edu.cn

†These authors contributed equally to this work

Nedd4 E3 proteins normally exist in the inactive steady state, suggesting that other domains of the protein outside HECT play a regulatory role to prevent non-physiological ubiquitination of E3s themselves, as well as their bona fide substrates. The C2 domains from Smurf1/2 and Nedd4/4L have been proposed to keep the HECT domain in a low-activity state where its ability for transthiolation and non-covalent Ub binding are impaired, and binding to Ca^{2+} /phospholipid or adaptors (e.g., Smad7, Cdh1), and Src-dependent phosphorylation could relieve the inhibitory C2-HECT interaction [28–33]. It was recently showed that Itch WW domains inhibit its ligase activity by blocking E2-E3 ligase transthiolation, and the auto-inhibitory WW-HECT interaction has also been observed in several Nedd4 E3s, though the underlying mechanisms are controversial [34–37]. Binding to PY containing targets or adaptors such as Nedd4 family-interacting protein 1/2 (Ndfip1/2) could disrupt the WW-HECT interaction [34,35,38,39]. In addition, the WW-HECT auto-inhibition could also be relieved upon JNK1-mediated phosphorylation in the proline-rich region (PRR) of Itch (Fig 1A) [37]. Nevertheless, although individual structures for C2, WW, and HECT domains have been solved separately, no structure

has been reported for any of the Nedd4 family proteins in the full-length or in an auto-inhibitory form. Elucidating the molecular mechanisms regulating the Nedd4 family E3 ligases should greatly advance the understanding of Nedd4 E3 function and offer therapeutic strategies for diseases related to Nedd4 deregulations.

Here, we solved the crystal structure of Itch in its inactive state, which provides an atomic picture for the auto-inhibited form of Nedd4 family E3s. The WW2 domain and the linker region connecting WW2 and WW3 (aa 351–381, referred to as L hereafter; Fig 1A) specifically bind to a hydrophobic surface opposite to the catalytic active site of the Itch HECT domain, thus allosterically locking HECT in a closed conformation. Mechanistically, the binding of WW2 and L restricts the inter-domain motion of the catalytic HECT domain. Ndfip1 binding to the WW domains including WW2 releases the auto-inhibited conformation of Itch. Interestingly, the JNK-1 phosphorylation-mediated Itch activation is also WW2 domain-dependent, likely due to an intramolecular interaction between phospho-PRR and WW2 and subsequent relief of the auto-inhibition. Forced expression of constitutively active forms of Itch designed based on our structural studies causes migration defects of neurons

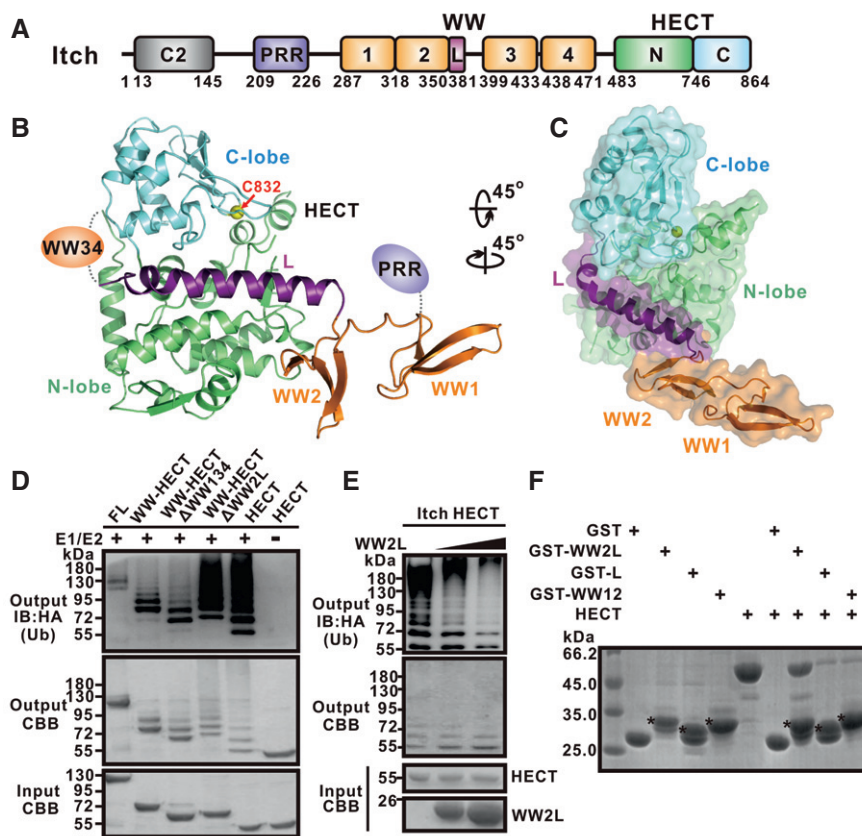


Figure 1. The closed conformation of Itch.

- A Domain organization of Itch.
 B Ribbon diagram representation of Itch Δ C2 structure. The coloring is the same as in panel (A). WW2 and the linker L pack with HECT. The catalytic Cys832 is indicated as a yellow sphere.
 C Surface diagram of Itch Δ C2. Cys832 is deeply buried in the N- and C-lobes of HECT. WW1 and WW2 form a compact supramodule.
 D Auto-ubiquitination assay of the full-length Itch and various fragments. The reaction was quenched at 15 min. CBB: Coomassie brilliant blue staining.
 E Itch HECT auto-ubiquitination assay with or without incubation of WW2L. The reaction was quenched at 15 min. CBB: Coomassie brilliant blue staining.
 F GST pull-down assay of GST-tagged WW2L, L and WW12 with HECT. GST and GST-tagged Itch proteins are indicated with asterisks.

in developing mouse cortex. Finally, we show that this WW2L-mediated regulation mechanism might be conserved in WWP1/2.

Results

Overall structure of the auto-inhibited Itch

Like most enzymes, Nedd4 E3s adopt a closed conformation in their steady state. Distinct from Smurf2 and Nedd4/Nedd4L, the C2 domain in Itch does not seem to play a key regulatory role in its ligase activity [28]. Consistent with that finding, our Itch auto-ubiquitination assay demonstrated that deletion of the C2 domain only slightly increased its E3 activity when compared with the full-length protein (Appendix Fig S1B). Pull-down assay further showed that the PW tandem (aa 143–478, containing both PRR and WW1–4, referred to as PW hereafter; Appendix Table S1) but not C2 robustly interacts with the HECT domain (Fig 1A and Appendix Fig S1C). To understand the molecular basis underlying the auto-inhibition of Itch, we determined the crystal structure of Itch Δ C2 (aa 143–864) at 2.6 Å resolution (Fig 1B and Table 1). The WW1, WW2, and the HECT domains in the Itch Δ C2 are well resolved, whereas the PRR, WW3, and WW4 domains could not be observed in the density map. WW2 and L pack

with the HECT domain. Specifically, WW2 interacts with the N-lobe, and L forms an α -helix and tucks into a shallow groove formed between the N- and C-lobes of HECT, away from the active site. Importantly, the structure reveals that the binding to WW2L locks the HECT domain in a closed conformation, with its active Cys832 (indicated by a yellow sphere) buried by the extensive interactions between N- and C-lobes of the HECT domain (Fig 1C). WW1 and WW2 interact with each other forming a compact supramodule, but WW1 does not directly contact the HECT domain (Fig 1B and C).

The auto-inhibited conformation of Itch revealed by the crystal structure was further confirmed by *in vitro* auto-ubiquitination assays (Fig 1D). The enzymatic activities of various forms of Itch mutants were tested in the presence or absence of E1 and E2. Although it was proposed that the PRR domain was involved in the regulation of the E3 activity [37], deletion of both C2 and PRR (WW-HECT) did not induce a dramatic increase of Itch activity in our hands (Fig 1D, lane 2). In line with the structural data, combinatorial deletion of C2, PRR, WW1, and WW34 (WW-HECT Δ WW134) had negligible impact on the auto-inhibition of Itch. In sharp contrast, deletion of both WW2 and L (WW-HECT Δ WW2L) dramatically increased Itch auto-ubiquitination, with an extent comparable to that of the isolated HECT domain (Fig 1D). A further direct binding inhibition assay showed that addition of purified WW2L inhibited the auto-ubiquitination of the Itch HECT catalytic domain in a dose-dependent manner (Fig 1E). Additionally, a GST pull-down assay showed that HECT could be robustly pulled down by GST-tagged WW2L, but only at the background levels by GST-WW12 or GST-L (Fig 1F). Taken together, our structural and biochemical data reveal that WW2L is the minimal unit responsible for keeping Itch in its auto-inhibited conformation.

Table 1. Data collection and refinement statistics.

	Itch Δ C2
Data collection	
Space group	P212121
Cell dimensions	
<i>a</i> , <i>b</i> , <i>c</i> (Å)	69.586, 77.084, 130.475
α , β , γ (°)	90.000, 90.000, 90.000
Wavelength (Å)	0.9754
Resolution (Å)	50.00–2.60 (2.64–2.60) ^a
<i>R</i> _{merge} (%)	7.1 (49.8)
Mean <i>I</i> / σ <i>I</i>	18.6 (3.0)
Completeness (%)	99.7 (100)
Redundancy	4.7 (4.8)
Refinement	
Resolution (Å)	48.03–2.60
No. reflections	21,846
<i>R</i> _{work} / <i>R</i> _{free}	21.4/26.2
No. atoms	
Protein	3,299
Water	46
B factors	
Protein	46.38
Water	27.45
R.m.s deviations	
Bond lengths (Å)	0.008
Bond angles (°)	1.059

^aValues in parentheses indicate the highest resolution shell.

The WW2L-HECT interface

Analysis of structural details at the WW2L-HECT interface shows that hydrophobic interactions make significant contributions to the binding, burying a total of ~1,500 Å² surface area (Fig 2A and B). Hydrophobic residues Tyr381, Ile380, Phe375, and Met372 from the C-terminus of L nestle into a hydrophobic cleft formed by Phe489, Val493, Phe559, Phe615, Leu742, Met746, and the aliphatic side chain of Lys490 from the N-lobe of HECT (Fig 2A), whereas Met569 from the N-lobe plugs into a small cavity formed by Trp325 from WW2 and Tyr358 from L (Fig 2B). These two core hydrophobic interactions physically integrate WW2L and the N-lobe into a compact complex. In addition, some charge–charge and hydrogen-bonding interactions further strengthen the WW2L-HECT interaction (Fig 2A and B). In agreement with the above structural analysis, mutations of some of these hydrophobic residues either from the N-lobe (F559E, M569A) or from L (Y381E) led to disrupted or severely impaired auto-inhibition of Itch (Figs 2C and EV1). Importantly, mutation of the signature Trp residue in WW2 (W325A, W347A), which is known to unfold a WW domain [40], also led to impaired auto-inhibition of Itch (Figs 2C and EV1), pointing to the critical role of WW2 in maintaining the auto-inhibited conformation of Itch.

WW2L-HECT packing locks Itch in the inactive state

Isolated Itch HECT (PDB ID: 3TUG) adopts a similar T-shaped “closed” conformation (Fig 3A) as WWP1, with its catalytic Cys far

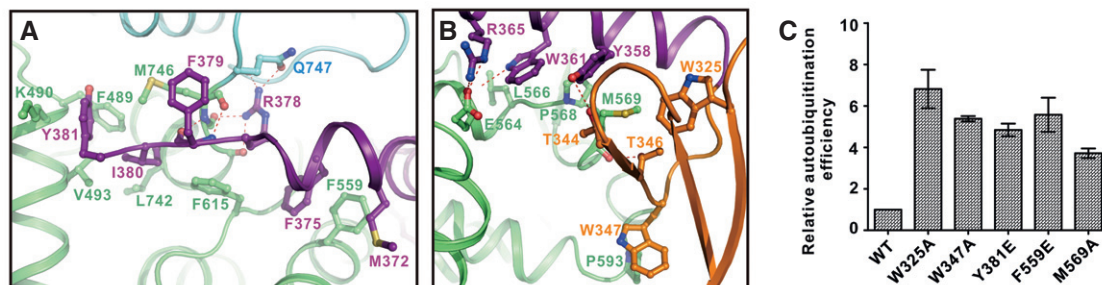


Figure 2. The WW2L and HECT interface in the inactive Itch.

- A, B Detailed interaction between WW2L and HECT. WW2L and HECT pack with each other through both hydrophobic and polar interactions. WW2 and L are colored as in Fig 1B. Key residues from WW2L involved in HECT interaction are drawn in the ball-and-stick model. Dotted lines denote hydrogen bonds and salt bridge interactions.
- C Auto-ubiquitination assay. Ubiquitination levels of Itch WT and mutants were quantified after a reaction time of 15 min using data shown in Fig EV1. Ubiquitination efficiencies were normalized to that of Itch WT and are plotted as the mean \pm SD of triplicate experiments.

away from the active site of a bound E2 [21]. Distinct from that of the auto-inhibited full-length Itch, this “closed” conformation is “pseudo-closed”, as the isolated HECT from WWP1 or Itch has high ligase activity, implying that the presence of E2-Ub will drive the “closed” conformation to an “open” one. Surprisingly, structural comparison revealed that Itch HECT in the WW2L-bound form adopts a similar apparent “closed” conformation as found in the HECT domain only structure (Figs 3A and EV2A). The main differences of the two structures are in the β 3, β 4, and the β 3- β 4 loop region of the N-lobe (referred to hereafter as Switch I, highlighted with a red dashed circle in Fig 3A), as well as the relative orientation of the two lobes. WW2L binding leads to a clockwise rotation of the C-lobe toward N-lobe by $\sim 7^\circ$, leading to further burial of the catalytic Cys832 in the N/C-lobe interface. However, such small conformational differences seem not sufficient to explain why WW2L binding locks HECT in a “real closed” state with a much lower ligase activity (Fig 1D and E).

More careful analysis of the WW2L-bound Itch HECT structure reveals that a number of residues from the N-lobe nested L make additional interactions with residues from the C-lobe of the HECT domain (Fig EV2B and C). For example, Tyr381 from L interacts with Met746 from the C-lobe and Arg378 from L forms a hydrogen bond with Gln747 from the C-lobe. These interactions presumably drive the $\sim 7^\circ$ rotation of the C-lobe toward the N-lobe in the auto-inhibited Itch structure (Fig 3A), and this inter-domain motion further promotes additional interactions between the two lobes of the HECT domain. For example, Tyr581 from the N-lobe forms hydrogen bonds with the main chains of Thr793 and Thr831 from the C-lobe in the auto-inhibited Itch. A striking outcome of the WW2L binding-induced inter-domain closure is formation of a strong hydrogen bond between His830 from the C-lobe and Glu639 from the N-lobe (Figs 3A and EV2C), which may lock the two lobes in a stable closed state (Fig EV2D). To test this hypothesis, we performed all-atom molecular dynamics simulations to compare the conformational dynamics of the Itch HECT domain (the inter-N/C-lobe motion in particular) in the HECT domain only and in the auto-inhibited conformations, using the isolated Itch HECT (3TUG) and the WW2L-bound Itch HECT structures as the starting conformation, respectively. The distance between E639 and H830 is monitored during the simulation, and the frequency of the potential

H-bond formation indicated by the distance between the two residues (below 3.2 Å) is calculated (Fig 3B). For the isolated Itch HECT domain, no H830-E639 H-bond formation is observed in the whole time course of the simulation (~ 42 ns; Fig 3B, blue). In contrast, H830-E639 form a dynamic H-bond if the WW2L-bound Itch HECT is used in the simulation (forming frequency $\sim 50\%$; Fig 3B, red). These data suggest that the presence of WW2L significantly stabilizes the formation of a hydrogen bond between H830 and E639.

Moreover, to achieve the active state, the closed WWP1/Itch HECT should undergo conformational changes with its C-lobe rotating out toward E2 to expose its active Cys for accepting Ub transferred from E2 [23]. However, by modeling the WW2L bound N-lobe of Itch HECT on to the E2-Ub-bound active Nedd4L HECT (PDB ID: 3JVZ), a severe steric clash could be observed between the C-lobe and L (Figs 3C and EV2E, highlighted with red dashed rectangle), indicating that binding of L to the N-lobe also prevents the rotation of the C-lobe to the active form. Since the WW2L binding site is far away from the E2 binding site on the N-lobe (Fig EV2E), WW2L is not likely to directly affect E2 binding, but instead regulates Itch’s activity through allosterically influencing the Ub transfer from E2.

To test the above structural analysis and results obtained from MD simulations, we first checked whether mutations that destabilize the N- and C-lobe interaction may cause an increase in Itch activity (Figs 3D and EV1). Satisfyingly, either E639A or the M746, Q747A mutation from the hinge region led to increased Itch auto-ubiquitination. A triple mutation of E639, M746, Q747A (referred to as EMQ/A hereafter) further increased the ligase activity. In line with these data, one-dimensional ^{19}F NMR measurement [41] revealed prominent chemical shift changes of Y381 to down-filed and Y581 to up-filed in EMQ/A compared with that in wild-type (WT) protein (Fig EV2F), indicating structural changes around the two residues upon introduction of the mutation (note that both Y381 and Y581 are key residues in keeping Itch in the inactive state; Figs 2A and EV2C).

Next, we compared Ub transfer from E2 to various forms of Itch. As expected, the auto-inhibited Itch full-length protein and the active Itch mutants (Itch Δ WW2L and Itch EMQ/A) possess comparable E2 binding properties as that of the isolated Itch HECT (Fig 3F). Compared with the full-length Itch, which has undetectable transthiolation, the active Itch Δ WW2L possesses significantly enhanced Ub transfer activity (Fig 3F and G). This result

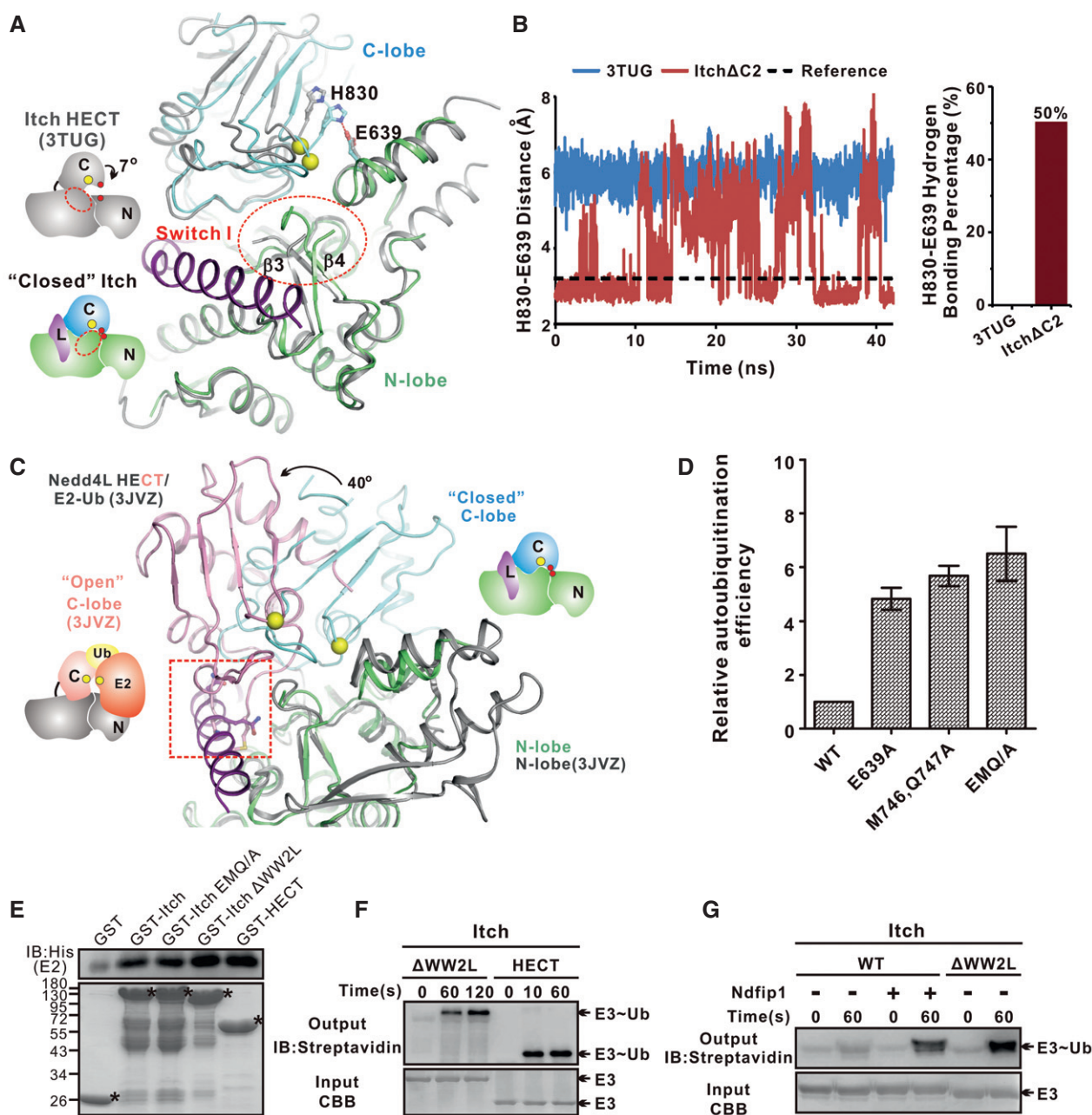


Figure 3. The WW2L allosterically inhibits Itch activity by blocking E2-E3 transthioleation.

- A** Superimposition of Itch HECT in the closed state with the apo-form (PDB ID: 3TUG). Switch I is highlighted with a red dashed circle. The catalytic Cys832 is indicated as a yellow sphere in the cartoon, whereas E639 and H830 are indicated as red spheres. For clarity, WW12 are omitted in the figure.
- B** Left: Molecular dynamics simulations of Itch HECT from different states. Time course of the distance between H830 and E639 from isolated Itch HECT (blue) and inactive Itch Δ C2 (red). Right: Percentage of H830-E639 H-bond formation during the time course of MD simulations. These results indicate that WW12L stabilizes the formation of H830-E639 hydrogen bond.
- C** Superimposition of Itch in the "closed" state and E2-Ub-bound Nedd4L HECT in the "open" state (PDB ID: 3JVZ). The catalytic sites in E3 and E2 are indicated as a yellow sphere in the cartoon, whereas E639 and H830 of Itch are indicated as red spheres. The steric clash between the C-lobe in the "open" state and L is highlighted with a red dashed rectangle. Interactions of L with the N- and C-lobes prevent the rotation of C-lobe to the active form.
- D** Auto-ubiquitination assay. Ubiquitination levels of Itch WT and mutants were quantified after a reaction time of 15 min using data shown in Fig EV1. Ubiquitination efficiencies were normalized to that of Itch WT and are plotted as the mean \pm SD of triplicate experiments.
- E** GST pull-down assay of GST-tagged Itch WT and mutants with His-E2. GST and GST-tagged Itch proteins are indicated with asterisks.
- F, G** Pulse-chase transfer of Ub from E2 to the indicated Itch proteins. E3-Ub thioester is indicated.

illustrates that the WW2L-bound Itch HECT domain is locked in an inactive state that prevents the E2-E3 transthioleation reaction instead of directly regulating E2 binding. Taken together, the above

structural, molecular dynamic simulations, and biochemical data demonstrated that the stabilization of the closed inter-N/C-lobe conformation as a result of WW2L binding is the origin of the

suppressed enzymatic activity of Itch, providing a mechanistic explanation of WW-mediated Itch auto-inhibition [35,37].

Ndfip1 binding or JNK1 phosphorylation activates Itch in a WW2-dependent manner

Next, we asked whether the WW2L-dependent auto-inhibition of Itch could be relieved through binding to its regulators or via post-translational modifications. The transmembrane adaptor protein Ndfip1 had been proposed to activate Itch through binding to its WW domains with three PY motifs located in its cytoplasmic N-terminus [35,38,39]. Auto-inhibition of Itch can also be relieved upon JNK1-mediated phosphorylation of S199, T222, and S232 in the PRR region of Itch [37]. We first confirmed that the Ndfip1 fragment containing all three PY motifs (aa 34–81, referred to as Ndfip1 hereafter) can promote Ub thioester formation and increase the auto-ubiquitination of Itch in a dose-dependent manner (Figs 3G and 4A). JNK-1 phosphorylation mimic mutants T222D, T222, S232D, or S199, T222, S232D (referred to as STS/D hereafter) can also relieve the auto-inhibition of Itch (Fig EV3A). We had tried to obtain high-quality crystals of Itch/Ndfip1 or Itch Δ C2/Ndfip1 complexes in order to understand how Ndfip1 binding activates Itch. However, our extensive attempts have failed presumably due to conformational flexibilities of the activated Itch.

To probe whether Ndfip1 binding destabilizes the intramolecular WW2L-HECT interaction by competing for WW2, we substituted His340 (a key residue for the WW domain to recognize the PY motif) from WW2 to Ala [42]. As shown in Fig 4B (right panel), compared with WT, the H340A mutation disrupted the Ndfip1 binding-induced activation of Itch WW-HECT, providing strong evidence that Ndfip1 binding releases the auto-inhibited conformation of Itch by displacing WW2 (and likely the following linker region) from the HECT domain. Interestingly, addition of the same amount of Ndfip1 could not enhance the catalytic activity of Itch WW-HECT Δ WW134 WT (Fig 4B, left panel), indicating that although WW1, 3, and 4 are not directly involved in the auto-inhibition of Itch, they may facilitate the Ndfip1-mediated displacement of WW2 from the HECT domain. It is interesting to note that the JNK-1 phosphorylation-mediated Itch activation is also WW2 dependent, as the H340A mutation significantly decreased the ligase activity of the phosphorylation mimic mutant PW-HECT Δ WW134 STS/D (Fig 4C). As WW domains can bind to “p[S/T]P” motifs [43], and all the three residues (S199, T222, and S232) in PRR are followed by a proline, it is plausible that JNK-1 phosphorylation leads to intramolecular interaction between PRR and WW2 and subsequently relieves the auto-inhibited conformation of Itch.

Multivalent interaction between Ndfip1 and Itch WW

We next confirmed that the specific Ndfip1 binding is mediated by Itch WW domains but not the HECT domain (Fig 4D and Appendix Fig S2). The isolated WW (WW1–4) binds to Ndfip1 with slightly higher affinity than the full-length protein (1.14 μ M versus 9.48 μ M), likely due to partial block of WW2 by HECT in the full-length Itch. Importantly, Ndfip1 and Itch HECT compete with each other for binding to WW domains (Fig EV3B), further supporting that the Ndfip1-WW interaction activates Itch by setting the catalytic HECT domain free. However, our extensive trials to obtain crystals

of Ndfip1/Itch WW complex failed, possibly due to the dynamic nature of the Itch-Ndfip1 complex (see below for more details).

As both Itch WW and Ndfip1 contain multiple protein–protein interaction modules, we asked whether all four WW domains in Itch and all three PY motifs in Ndfip1 are required for activating Itch, and how they interact with each other. By mutating one signature Trp residue in each of the four WW domains, which is known to unfold a WW domain [40], we were able to dissect the contribution of each WW domain to Ndfip1 binding. We found that each individual WW of Itch interacted with Ndfip1 with a relative weak affinity, and that tandem WW domains (WW12 or WW34) showed a significantly increased binding avidity through synergistic interactions. Consistent with this result, disrupting any single WW domain only slightly weakened the interaction between Ndfip1 and the Itch WW domains (Fig 4D and Appendix Fig S3). As a negative control, the substitution of W361 from L with Alanine did not cause any change in the WW-Ndfip1 interaction. Similarly, the mutation of any single PY motif only slightly impaired Itch binding and all three PY motifs of Ndfip1 are required for efficient Itch activation (Figs 4D and EV3C, and Appendix Fig S4), consistent with previous results [35,38].

How can three PY motifs of Ndfip1 interact with four WW domains? The analytical gel filtration analysis showed that Itch WW eluted as a broad peak with some degree of aggregation (Fig EV3D). Besides, none of the eight Trp side-chain amides could be detected in the ^{15}N , ^1H -HSQC spectrum of Itch WW (Fig 4E), indicating that the protein is highly heterogeneous or undergoes intermediate conformational equilibrium. Similar phenomena have been observed in Smurf1 and Smurf2, where the WW1 of Smurf1 and WW2 of Smurf2 play a role in protein oligomerization and aggregation [31,44]. Binding to Ndfip1 improved the conformational homogeneity of WW, as we could observe a gradual appearance of Trp side-chain amide peaks of Itch WW in a dose-dependent manner (Fig 4E). In the presence of a saturating amount of Ndfip1, all eight Trp side-chain amide peaks can be detected. Next, through mutation of each Trp at a time, the eight Trp side-chain amides were assigned (Fig EV3E). Combined with the data shown in Fig EV3F where the contribution of each single PY motif in Ndfip1–Itch interaction was assessed, two key points emerged. First, WW2 and L mediate the conformational equilibrium of Itch WW, as either the W325A mutation which induced WW2 unfolding or W361A mutation from L significantly improved the Itch WW conformational homogeneity, as indicated by appearance of Trp side-chain amide peaks even without pre-incubation of Ndfip1. Second, PY2 and PY3 coordinate for Itch WW34 binding, whereas PY1 binds to WW1 or WW2 with no selectivity. WW1 or WW3 only recognize a single PY motif in Ndfip1 ($N \sim 1$), whereas WW2 or WW4 could interact with two PY motifs in Ndfip1 ($N \sim 0.5$; Appendix Fig S2). Taken together, our ITC and NMR data suggested that the interaction between Itch WW and Ndfip1 is a multivalent interaction, which requires all three PY motifs from Ndfip1 and multiple WW domains from Itch, and the remaining unoccupied WW can be used for recruitment of diverse targets.

Itch WW simultaneously interacts with Ndfip1 and JunB

The WW domain is the main mediator of substrate recognition by Nedd4 E3s. We therefore asked the question whether Ndfip1 binding-mediated activation of Itch affects target recognition (such as JunB). We found that JunB weakly binds to isolated WW1 and

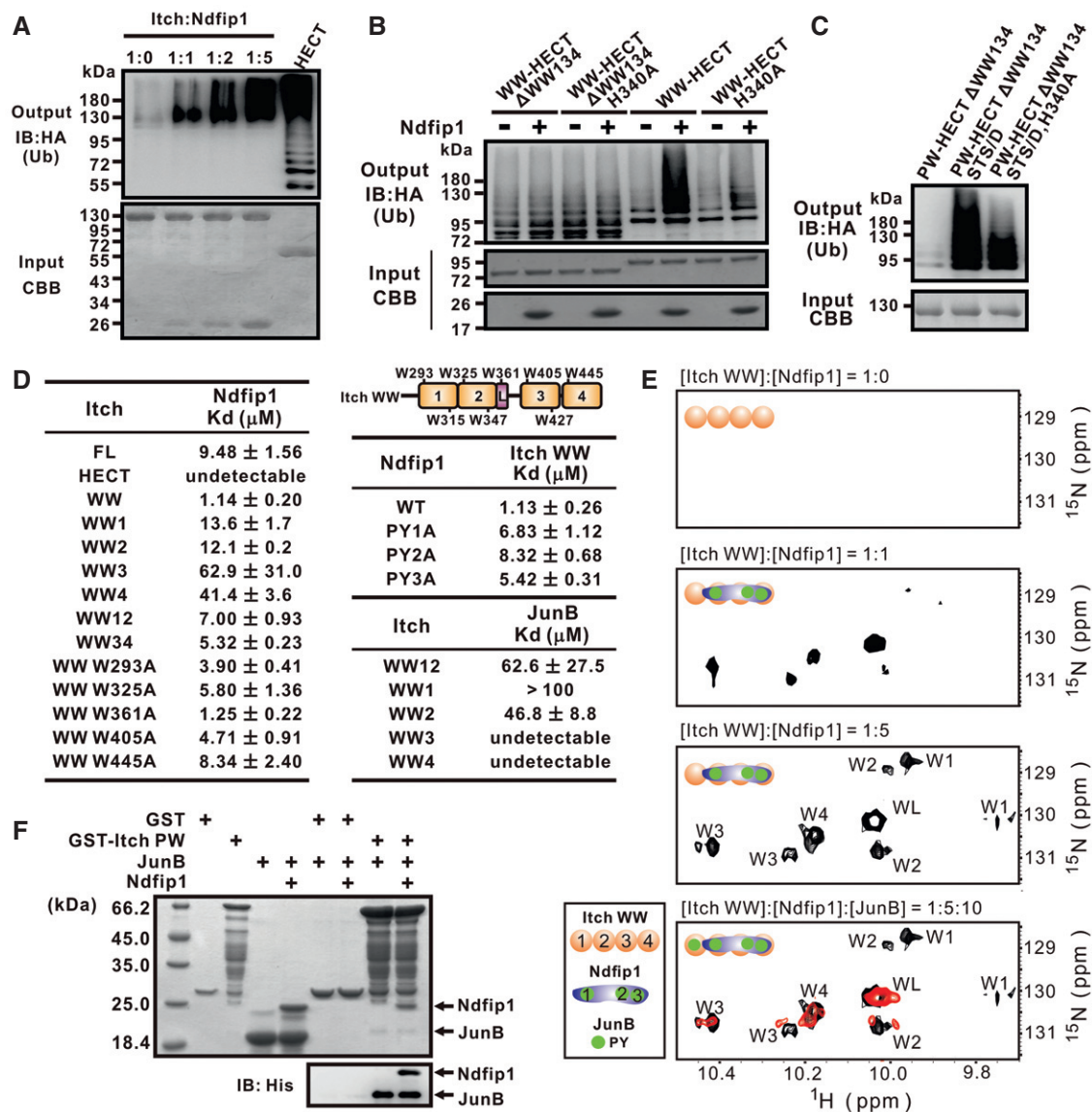


Figure 4. Multivalent Ndfip1-WW interaction activates Itch by displacing WW2 from the HECT domain.

- A Itch auto-ubiquitination assay with or without indicated amount of Ndfip1. Ndfip1 activates Itch in a dose-dependent manner.
 B, C Auto-ubiquitination assay of various Itch proteins with or without incubation of Ndfip1. (B) Ndfip1 activates Itch through binding to WW2, and WW134 are also required for Ndfip1-mediated Itch activation. (C) Itch activation induced by the JNK-1 phosphorylation mimic STS/D mutation is also WW2 dependent.
 D Summary of the ITC-based measurement of the binding between various Itch constructs and Ndfip1 or JunB fragments in Appendix Figs S2–S5.
 E Selected region of the ^{15}N , ^1H -HSQC spectra of Itch WW (~ 0.1 mM) with indicated molar ratios of Ndfip1 in the absence (black) and presence of JunB (red).
 F GST pull-down assay. GST-tagged Itch PW but not the GST control could simultaneously interact with both Ndfip1 and JunB.

WW2 domains of Itch (Fig 4D and Appendix Fig S5). Addition of JunB to ^{15}N -labeled Itch WW pre-saturated with Ndfip1 led to peak disappearance of Trp side-chain amide peaks from WW1 and weaker peaks from WW2 (Fig 4E), indicating that in the Ndfip1-bound state, the recruitment of JunB is mediated at least in part by WW1. Moreover, GST pull-down assay showed that the presence of a saturating amount of Ndfip1 did not affect the binding avidity between Itch PW and JunB, indicating that Itch could simultaneously interact with the activator Ndfip1 and target JunB (Fig 4F). An attractive hypothesis is therefore that, when Itch is activated by its

adaptor Ndfip1 (dependent on WW2), the WW1 domain can recruit the substrate JunB for Ub transfer.

Activation of Itch promotes neuronal migration in the developing mouse neocortex

Beyond the essential function in the control of immune system, Itch is also implicated in other biological processes, including development, tumorigenesis, and stress responses [45,46]. Most of these findings were made in an Itch-deficient context, for example, the

Itch^{-/-} Itchy mice. Itchy mice have fatal autoimmune disease with inflammation of the skin and intestine, and lymphocyte infiltration of lungs, liver, kidneys, and heart [11]. Whereas Itch-deficient patients not only have syndromic multisystem autoimmune disease but also are delayed in gross motor skills and cognitive skills [9]. In addition, Itch is strongly expressed in human neurons (Protein Atlas; see Web Resources) and the mouse brain, although no obvious brain functional defect was observed in the Itch^{-/-} Itchy mice [11,47]. To address whether the Itch ligase activity is of functional significance in brain development, we employed the developing mouse neocortex as an *in vivo* model and performed *in utero* electroporation at embryonic day 14.5 (E14.5). Either GFP-tagged WT, the constitutively active EMQ/A mutant, or the JNK1 phosphorylation mimic STS/D mutant of Itch was individually transfected into cortical regions of mouse embryos. 3 days post-transfection, neurons migrated properly to the cortical plate where they evenly distributed in control brains electroporated with constructs expressing GFP or Itch WT only (Fig 5A and B). In contrast, most neurons derived from progenitors electroporated with the construct expressing EMQ/A-Itch, the constitutively active form of Itch designed based on structural analysis (Fig 3D), had left the intermediate zone (IZ) and migrated to the upper part of the cortical plate (Fig 5A and B). Consistent with the fact that both EMQ/A and STS/D mutations activate Itch constitutively *in vitro* (Figs 3D and EV3A) [37], we also observed that overexpression of the construct expressing STS/D-Itch led to neuronal overmigration (Fig 5A and B). These results indicate

that both EMQ/A and STS/D mutations aberrantly activate Itch *in vivo* and lead to overmigrations of cortical neurons, which is linked to profound neurodevelopmental and cognitive disorders [48]. Itchy mice did not show obvious defect in brain development or function, possibly due to potential redundant functions of other Nedd4 family members, as it has been shown that certain Nedd4 members may share the same targets [5].

WW2L-mediated auto-inhibition in WWP1/2

All the Nedd4 family E3 ligases including Itch share the same architecture containing a C2, two to four WW, and a HECT from their N- to C-termini (Appendix Fig S1A). We then asked whether the WW2L-mediated auto-inhibition of the HECT is conserved in other Nedd4 family members. Primary sequence analysis of the Nedd4 family proteins revealed that the WW2L organization also exists in WWP1 and WWP2 (Appendix Fig S6A), but not in other members. Importantly, the amino acid sequence conservation map of WW2L and HECT of Itch and WWP1/2 showed that the key residues involved in Itch WW2L-HECT binding (indicated with cyan triangle in Appendix Fig S6A and red circle in Appendix Fig S6B) are highly conserved (Fig EV4A), implying that the WW2L domain of WWP1/2 might also play a regulatory role in their catalytic activities. In line with this hypothesis, deletion of WW2L significantly enhanced auto-ubiquitination of WWP2 compared to WT (Fig EV4B). Similar to Itch, the C2 domain of WWP2 does not play a

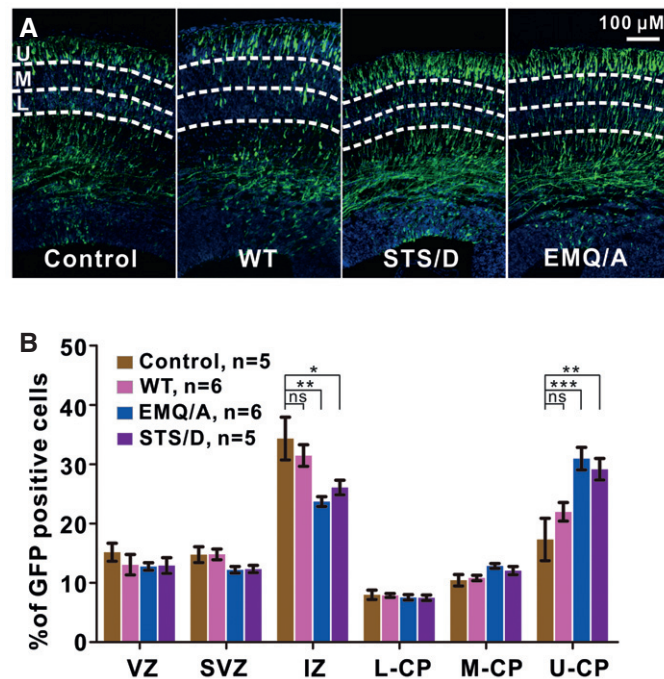


Figure 5. Aberrant activation of Itch leads to migration defects of cortical neurons during neurogenesis.

A *In utero* electroporation of GFP-tagged WT, the constitutively active EMQ/A mutant, or the JNK1 phosphorylation mimic STS/D mutant of Itch at the embryonic day 14.5 (E14.5). Electroporation of the constructs expressing EMQ/A and STS/D led to neuronal overmigration. U, M, and P: upper, middle, and lower cortical plate, respectively.
 B Statistics of neurons in different cortical subregions ($n = 5-6$) shown in panel (A). VZ: ventricular zone; SVZ: subventricular zone; IZ: intermediate zone; U-CP, M-CP, and L-CP: upper, middle, and lower cortical plate, respectively. Data are presented as mean \pm SEM; ns, not significant, * $P < 0.05$, ** $P < 0.01$, and *** $P < 0.001$ using one-way ANOVA with uncorrected Fisher's LSD test.

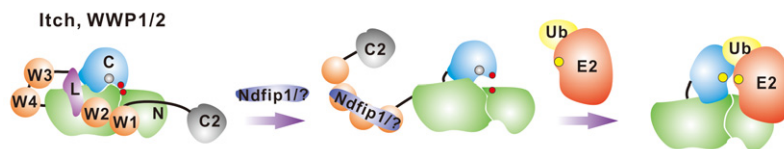


Figure 6. Model of the regulation and activation of Itch.

WW domains play an inhibitory role in Nedd4 E3 Itch (likely WWP1/2 as well) by directly binding to the HECT domain, and allosterically lock E3 in the closed state by impairing E2-E3 transthiolation. Itch could be activated via multivalent PY-WW interactions with adaptors (such as Ndfip1) and thus promote temporal-specific target ubiquitination.

key role in regulating its ligase activity. Although we could not get recombinant protein of the full-length protein, the truncated Δ C2 form of WWP1 possessed barely any activity as its counterparts Itch and WWP2 do, and deletion of WW2L dramatically increased its ligase activity (Fig EV4B), indicating that the mechanism of auto-inhibition of WWP1/2 might be similar to Itch. Consistent with the *in vitro* ubiquitination assays, GST pull-down results showed that WWs from WWP1/2 interacted with their HECTs with high affinity (Fig EV4C and D).

Discussion

WW-mediated auto-inhibition of Nedd4 E3 Itch

It is increasingly clear that each of the Nedd4 family E3s adopts an auto-inhibited state in which a region of each E3 outside its catalytic HECT domain somehow keeps the enzyme in their low-activity state. We provided the atomic structure of an auto-inhibited Nedd4 member Itch and demonstrated that Itch WW domains play an inhibitory role by directly binding to the HECT domain and allosterically lock the E3 in the inactive state by impairing E2-E3 transthiolation (Fig 6). This WW-mediated auto-inhibition mechanism might also exist in WWP1/2.

Detailed structural comparison further revealed that the WW2L binding site on Itch HECT and the C2 binding site on Smurf2 HECT are partially overlapped with the non-covalent Ub binding site on Nedd4 HECT (Fig EV5) [24,28,29,49]. Amino sequence alignment of all nine Nedd4 family members revealed that most residues in the HECT domains involved in WW2L binding in Itch HECT are highly conserved in WWP1/2, and less in other Nedd4 E3s (Appendix Fig S6B). Most residues involved in the C2 binding in Smurf2 HECT are more conserved in Smurf1 and Nedd4/4L, and these HECT domains have been demonstrated to bind to their respective C2 domain [28,29]. Thus, this versatile hydrophobic surface on each of the HECT might be commonly utilized in C2 or WW binding in this E3 family members.

When this manuscript is under revision, Chen *et al* [50] provided the auto-inhibited structure of WWP2, in which WW2L interacts with the HECT domain in a way highly similar to that seen in Itch presented in this study, further supporting the proposed auto-inhibition model for Itch and WWP1/2.

WW-mediated specific activation of Itch

Though some may play a redundant role in certain cellular events, the various Nedd4 family members exhibit unique functions [5].

Due to the generally low selectivity between WW domains and single PY motif-containing targets, specific activation of Nedd4 E3s is vital to avoid non-physiological crosstalk. For Itch (likely WWP1/2 as well), due to the strong binding between WW2L and HECT, single PY motif-containing targets cannot activate E3 by directly competing with HECT for WW2. C2-mediated membrane targeting controls the subcellular localization of E3, but cannot activate it either. Tandem WW domains of Itch act as a convergent point for efficient ligase activation and target recognition: Only when multiple PY containing adaptors (such as Ndfip1) come, Itch could be activated via multivalent intermolecular PY-WW interactions with adaptors and thus promote temporal-specific target ubiquitination. For example, the Itch-mediated temporal degradation of JunB happens after T activation [39]. T-cell stimulation promotes Ndfip1 expression. The Ndfip1-Itch interaction leads to relocalization and activation of Itch near the plasma membrane and subsequently induces ubiquitination and turnover of JunB, whereas Itch remained within the cytoplasmic vesicles in cells lacking Ndfip1. Alternatively, activation of JNK1 after T-cell stimulation leads to phosphorylation of Itch PRR region, which generates “p[S/T]” motifs to bind to the WW domains and concomitant displacement of WW2 from the HECT domain of Itch [14,37]. Since the key residues from WW2L of Itch involved in HECT binding are evolutionarily conserved from mouse to human (Appendix Fig S6A), the Ndfip1- and JNK1-mediated Itch activation found in mouse immune system is likely conserved in human as well. Moreover, the JNK1 sites found in Itch PRR are not found in other Nedd4 family E3s, indicating that the upstream JNK1 signal may only activate Itch but not other Nedd4 E3s. In addition to the WW domain-based activation, Itch and WWP1/2 may also be activated in a L-dependent way, such as through phosphorylation on L in WWP2 [50].

Materials and Methods

Protein expression and purification

Various mouse Itch fragments (Fig 1 and Appendix Table S1), human Ndfip1 fragment (aa 34–81), human JunB fragment (aa 166–194), and various fragments from human WWP1/2 (Fig EV4) were individually cloned into pGEX-6P-1 or a modified version of the pET32a vector [51], with the resulting protein containing a GST or Trx-His₆ tag in its N-terminus. All of the mutations were created through standard PCR-based mutagenesis method and confirmed by DNA sequencing. Recombinant proteins were expressed in *Escherichia coli* BL21 (DE3) host cells at 16°C and were purified by using

GST or Ni²⁺-NTA agarose affinity chromatography followed by size-exclusion chromatography. Uniformly ¹⁵N-labeled Itch WW WT or various mutants were prepared by growing bacteria in M9 minimal medium using ¹⁵NH₄Cl (Cambridge Isotope Laboratories Inc.) as the sole nitrogen source.

In vitro ubiquitination assay

For the *in vitro* auto-ubiquitination assay, 800 nM Nedd4 family E3s or their truncated forms were incubated with 60 nM E1 (UBE1), 400 nM E2 (UBCH5A), and 20 μM HA-ubiquitin in 50 μl volumes containing 50 mM Tris (pH 7.5), 5 mM MgCl₂, 1 mM DTT, and 3 mM ATP. After incubated in 37°C for indicated time, the reaction mixtures were resolved by SDS-PAGE, stained with Coomassie brilliant blue (CBB), and used for immunoblotting. For Ndfip1-mediated activation of Nedd4 E3s, E3s were pre-incubated with Ndfip1 at ten molar ratios or an indicated amount. The reaction time for Ndfip1-mediated activation of Nedd4 E3s, and auto-ubiquitination of various E3 mutants was 30 min or indicated time.

Ub transthiolation assay

The ubiquitin pulse-chase assay was performed in two steps. First, 5 μM UBCH5A was reacted with 0.25 μM E1 and 10 μM biotinylated ubiquitin (Boston Biochem) in 50 mM Tris (pH 7.6), 250 mM NaCl, 8.3 mM MgCl₂, 1.7 mM ATP, and 3.3 μg ovalbumin for 30 min at 37°C. Reactions were quenched by diluting four-fold with 25 mM HEPES (pH 7.5), 100 mM NaCl, and 25 mM EDTA. Then, E2-Ub was mixed with various Itch proteins on ice to initiate a single round of substrate ubiquitination. Reactions were quenched with an equal volume of Laemmli buffer at indicated time, and ubiquitylated products were resolved on SDS gels and detected using horseradish peroxidase (HRP)-conjugated streptavidin (Abcam, Cat#: ab7403) for immunoblotting.

Immunoblotting

The reaction mixtures were subjected to SDS-PAGE and then transferred to a 0.45 μM PVDF membrane (Millipore), which was blocked using 3% BSA in TBST [20 mM Tris-HCl (pH 7.4), 137 mM NaCl and 0.1% Tween 20] buffer at room temperature for 1 h; this was followed by incubation with HA (ABclonal, Cat#: AE008) or His (Proteintech, Cat#: 66005-l-1g) antibody at a 1/2,000 dilution at 4°C overnight. Membranes were washed three times with TBST buffer, incubated with horseradish peroxidase (HRP)-conjugated goat anti-mouse antibody (ABclonal, Cat#: AS014) or anti-rabbit antibody (ABclonal, Cat#: AS003), and visualized on a LAS3000 Chemiluminescence Imaging System.

GST pull-down assay

For the GST pull-down assay, GST or GST-tagged various Nedd4 E3 proteins (4 nmol) was first loaded onto GSH-Sepharose 4B slurry beads and then incubated with 12 nmol potential binding proteins in a 500-μl assay buffer [containing 50 mM Tris (pH 8.0), 100 mM NaCl, 1 mM DTT, and 1 mM EDTA] for 1 h at 4°C. After three times washing, proteins captured by affinity beads were eluted by boiling, resolved by 12% SDS-PAGE, and detected by CBB.

Crystallography

Freshly purified ItchΔC2 was concentrated to 12 mg/ml, and the crystals were grown by the hanging drop vapor diffusion method at 16°C in a reservoir solution containing 50 mM citric acid (pH 5.5), 50 mM Bis-Tris propone, and 16% PEG3350. The crystals were soaked in crystallization solution containing 15% glycerol for cryoprotection. The diffraction data of the crystals were collected at the NCPSS (National Center for Protein Sciences Shanghai) and SSRF (Shanghai Synchrotron Radiation Facility) beamline BL18U at a wavelength of 0.9754 Å. The data were processed and scaled using HKL3000. The phase problem of ItchΔC2 was solved by molecular replacement using the Itch HECT structure (PDB ID: 3TUG) as the search model against the 2.6-Å resolution dataset. The initial model was further rebuilt, adjusted manually with COOT [52] and refined by the phenix.refine program of PHENIX [53]. The final model had 95.7% of the residues in the favored region of the Ramachandran plot with no outliers. The final refinement statistics are summarized in Table 1.

Data availability

Coordinates of the crystal structure of ItchΔC2 have been deposited in the Protein Databank under the accession code 5XMC.

Molecular dynamics simulations

Isolated Itch HECT (3TUG) and the WW2L-bound Itch HECT (ItchΔC2, this study) structures were used as the initial structures for MD simulations. The missing regions in both structures were added with ModLoop and by structural alignments with other homology structures (HECT domain from Smurf2 and Nedd4L, PDB code 1ZVD and 3JVZ, respectively). The resulted systems were processed with VMD [54] to add the missing hydrogens, solvate in a water box, and add counterions to neutralize the system with 0.15 M ion concentration. The MD simulations were performed with NAMD package [55], and the CHARMM36 all-atom force field with CMAP correction [56] was used for all simulations. A 12 Å cutoff was used for short-range non-bounded interactions, and Particle Mesh Ewald summation was used for long-range electrostatic interaction calculation. At first, a multiple step energy minimization process was carried out to remove potential clashes. Then, the systems were equilibrated for 10 ns. The resulted systems were simulated for about 40 ns, and the results were analyzed by VMD program. During the simulations, the temperature was maintained at 300 K by Langevin thermostat and the pressure was maintained at 1 atm by Langevin piston barostat. The SHAKE algorithm was used to allow 2-fs time step in the simulations.

Expression and purification of ¹⁹F labeled proteins

The L-4-trifluoromethyl phenylalanine (tfmF) site-specific labeled protein was overexpressed using a double-plasmid system. An orthogonal tRNA_{CUA}/tRNA synthetase system was used to incorporate ¹⁹F-labeled unnatural amino acid. Briefly, to perform site-specific labeling, the DNA fragment of Itch was designed by replacing the natural base at the desired sites by TAG codon. A modified pEVOL-tfmFRS plasmid to express tRNA_{CUA} and

tfmF-specific aminoacyl-tRNA was co-transformed with the TAG-carrying plasmid into BL21 (DE3) [57]. The transformed cells were incubated with LB media in the presence of tfmF at 37°C. The bacteria were induced with 0.02% L-arabinose and 0.3 mM IPTG and then transferred to 16°C for 20 h. The bacteria were harvested and purified by Ni-NTA affinity chromatography and size-exclusion chromatography as for wild-type Itch proteins.

¹⁹F NMR spectra measurements

All one-dimensional ¹⁹F NMR spectra measurements were performed at 25°C on an Agilent 500 MHz spectrometer equipped with a HFT probe, and the observation channel was tuned to ¹⁹F (470.2 MHz), with 10,240 free induction decay (FID) accumulations in every 3-s recycling delay. One-dimensional ¹⁹F spectra were acquired with one pulse program with 90° pulse width of 12.45 μs and power at 57 w. The spectra width was 60 ppm, and offset was -62 ppm. ¹⁹F chemical shifts were referenced to an external standard, tfmF (-62.38 ppm). The data were processed and plotted with an exponential window function (line broadening = 20 Hz) using ACD/NMR Processor Academic Edition software (ACD/Labs).

ITC measurements

ITC measurements were performed on an ITC200 Micro calorimeter (MicroCal) at 25°C. All of the protein samples were dissolved in a buffer containing 50 mM Tris (pH 8.0), 1 mM EDTA, 1 mM β-mercaptoethanol, and 100 mM NaCl. The titrations were carried out by injecting 40 μl aliquots of Ndfip1 proteins or JunB (~0.5 mM) into various Itch fragments (~0.05 mM) at time intervals of 2 min to ensure that the titration peak returned to the baseline. The titration data were analyzed using the program Origin 7.0 and fitted by the one-site binding model.

NMR experiments

¹⁵N-labeled Itch WW samples were concentrated to ~0.1 mM in 50 mM PBS (pH 6.8, with 1 mM EDTA and 100 mM NaCl). NMR spectra were acquired at 25°C on a Varian Inova 800 MHz spectrometer (A800) at NCPSS.

In utero electroporation

In utero electroporations were carried out as described previously [58]. Briefly, timed pregnant C57BL/6J mice were anesthetized, and then, the uterine horns were exposed. DNA solution (1.5 μg/μl) was injected into the lateral ventricles. Embryonic head was held with platinum electrodes (7 mm, BTX). Five 50 ms pulses of 35 mV with 950 ms intervals were applied with an electroporator (BTX, ECM830). After electroporation, uterine horns were placed back into abdominal cavity and the wounds were sutured. Embryonic brains were analyzed 3 days later. All procedures were carried out in accordance with institutional guidelines.

Immunohistochemistry

Embryonic brains (E17.5) were fixed by 4% paraformaldehyde in PBS overnight at 4°C, followed by cryoprotection in 30% sucrose. After

sinking into the bottom, brains were embedded and sectioned at 14 μm using cryostat microtome (Leica Micro-systems). Brain sections were permeabilized and then incubated with blocking buffer (5% goat serum plus 0.1% Triton X-100 plus 5% BSA in PBS) for 1 h at room temperature. Incubation of primary antibody (chicken anti-GFP, 1:1,000, Abcam, Cat#: ab13970) was then performed at 4°C overnight. After washing with PBS, sections were incubated with fluorescence-conjugated secondary antibody (Invitrogen, Cat#: A11039).

Imaging and quantification

All images were acquired using the Olympus FV1000 confocal microscope system. For quantification, sections from 5 to 6 brains were analyzed in double-blinded fashion. Cortical subregions were distinguished according to DAPI-stained nucleus. All statistical analyses were performed using GraphPad Prism 5. *P*-values **P* ≤ 0.05 were considered statistically significant.

Expanded View for this article is available online.

Acknowledgements

We thank Dr. Mingjie Zhang for valuable discussions; Drs. Ceshi Chen, Lingqiang Zhang, and Jing Fang for WWP1/2 and JunB genes; the staff of NMR A800 and beamlines BL17U1 and BL18U at NCPSS and SSRF for data collection. This work was supported by grants from the Ministry of Science and Technology of the People's Republic of China (2014CB910201), the National Natural Science Foundation of China (31670730, 31422015, 31270778), the Program for New Century Excellent Talents in University (NCET-12-0129), and the Shanghai Municipal Education Commission (14SG06) to W.W.

Author contributions

KZ, ZS, XC, CT, JL, YX, and WW designed the research and analyzed data. KZ, ZS, XC, YC, LC, WY, ZW, and PS performed experiments. WW drafted the manuscript, and all authors commented on it. WW coordinated the project.

Conflict of interest

The authors declare that they have no conflict of interest.

References

- Hershko A, Ciechanover A (1998) The ubiquitin system. *Annu Rev Biochem* 67: 425–479
- Nalepa G, Rolfe M, Harper JW (2006) Drug discovery in the ubiquitin-proteasome system. *Nat Rev Drug Discov* 5: 596–613
- Buetow L, Huang DT (2016) Structural insights into the catalysis and regulation of E3 ubiquitin ligases. *Nat Rev Mol Cell Biol* 17: 626–642
- Berndsen CE, Wolberger C (2014) New insights into ubiquitin E3 ligase mechanism. *Nat Struct Mol Biol* 21: 301–307
- Rotin D, Kumar S (2009) Physiological functions of the HECT family of ubiquitin ligases. *Nat Rev Mol Cell Biol* 10: 398–409
- Bernassola F, Karin M, Ciechanover A, Melino G (2008) The HECT family of E3 ubiquitin ligases: multiple players in cancer development. *Cancer Cell* 14: 10–21
- Chen C, Matesic LE (2007) The Nedd4-like family of E3 ubiquitin ligases and cancer. *Cancer Metastasis Rev* 26: 587–604
- Fang D, Elly C, Gao B, Fang N, Altman Y, Joazeiro C, Hunter T, Copeland N, Jenkins N, Liu YC (2002) Dysregulation of T lymphocyte function in

- itchy mice: a role for Itch in TH2 differentiation. *Nat Immunol* 3: 281–287
9. Lohr NJ, Molleston JP, Strauss KA, Torres-Martinez W, Sherman EA, Squires RH, Rider NL, Chikwava KR, Cummings OW, Morton DH et al (2010) Human ITCH E3 ubiquitin ligase deficiency causes syndromic multisystem autoimmune disease. *Am J Hum Genet* 86: 447–453
 10. Matesic LE, Haines DC, Copeland NG, Jenkins NA (2006) Itch genetically interacts with Notch1 in a mouse autoimmune disease model. *Hum Mol Genet* 15: 3485–3497
 11. Perry WL, Hustad CM, Swing DA, O'Sullivan TN, Jenkins NA, Copeland NG (1998) The itchy locus encodes a novel ubiquitin protein ligase that is disrupted in a18H mice. *Nat Genet* 18: 143–146
 12. Mueller DL (2004) E3 ubiquitin ligases as T cell anergy factors. *Nat Immunol* 5: 883–890
 13. Liu YC (2004) Ubiquitin ligases and the immune response. *Annu Rev Immunol* 22: 81–127
 14. Gao M, Labuda T, Xia Y, Gallagher E, Fang D, Liu YC, Karin M (2004) Jun turnover is controlled through JNK-dependent phosphorylation of the E3 ligase Itch. *Science* 306: 271–275
 15. Chang L, Kamata H, Solinas G, Luo JL, Maeda S, Venuprasad K, Liu YC, Karin M (2006) The E3 ubiquitin ligase itch couples JNK activation to TNF α -induced cell death by inducing c-FLIP(L) turnover. *Cell* 124: 601–613
 16. Rossi M, De Laurenzi V, Munarriz E, Green DR, Liu YC, Vousden KH, Cesareni G, Melino G (2005) The ubiquitin-protein ligase Itch regulates p73 stability. *EMBO J* 24: 836–848
 17. Rossi M, Aqeilan RI, Neale M, Candi E, Salomoni P, Knight RA, Croce CM, Melino G (2006) The E3 ubiquitin ligase Itch controls the protein stability of p63. *Proc Natl Acad Sci USA* 103: 12753–12758
 18. Qiu L, Joazeiro C, Fang N, Wang HY, Ely C, Altman Y, Fang D, Hunter T, Liu YC (2000) Recognition and ubiquitination of Notch by Itch, a hect-type E3 ubiquitin ligase. *J Biol Chem* 275: 35734–35737
 19. Rathinam C, Matesic LE, Flavell RA (2011) The E3 ligase Itch is a negative regulator of the homeostasis and function of hematopoietic stem cells. *Nat Immunol* 12: 399–407
 20. Ingham RJ, Gish G, Pawson T (2004) The Nedd4 family of E3 ubiquitin ligases: functional diversity within a common modular architecture. *Oncogene* 23: 1972–1984
 21. Verdecia MA, Joazeiro CA, Wells NJ, Ferrer JL, Bowman ME, Hunter T, Noel JP (2003) Conformational flexibility underlies ubiquitin ligation mediated by the WWP1 HECT domain E3 ligase. *Mol Cell* 11: 249–259
 22. Ogunjimi AA, Briant DJ, Pece-Barbara N, Le Roy C, Di Guglielmo GM, Kavsak P, Rasmussen RK, Seet BT, Sicheri F, Wrana JL (2005) Regulation of Smurf2 ubiquitin ligase activity by anchoring the E2 to the HECT domain. *Mol Cell* 19: 297–308
 23. Kamadurai HB, Souphron J, Scott DC, Duda DM, Miller DJ, Stringer D, Piper RC, Schulman BA (2009) Insights into ubiquitin transfer cascades from a structure of a UbcH5B approximately ubiquitin-HECT(NEDD4L) complex. *Mol Cell* 36: 1095–1102
 24. Maspero E, Valentini E, Mari S, Cecatiello V, Soffientini P, Pasqualato S, Polo S (2013) Structure of a ubiquitin-loaded HECT ligase reveals the molecular basis for catalytic priming. *Nat Struct Mol Biol* 20: 696–701
 25. Huang L, Kinnucan E, Wang G, Beaudenon S, Howley PM, Huijbregtse JM, Pavletich NP (1999) Structure of an E6AP-UbcH7 complex: insights into ubiquitination by the E2-E3 enzyme cascade. *Science* 286: 1321–1326
 26. Lorenz S, Cantor AJ, Rape M, Kuriyan J (2013) Macromolecular juggling by ubiquitylation enzymes. *BMC Biol* 11: 65
 27. Attali I, Tobelaim WS, Persaud A, Motamedchaboki K, Simpson-Lavy KJ, Mashahreh B, Levin-Kravets O, Keren-Kaplan T, Pilzer I, Kupiec M et al (2017) Ubiquitylation-dependent oligomerization regulates activity of Nedd4 ligases. *EMBO J* 36: 425–440
 28. Wiesner S, Ogunjimi AA, Wang HR, Rotin D, Sicheri F, Wrana JL, Forman-Kay JD (2007) Autoinhibition of the HECT-type ubiquitin ligase Smurf2 through its C2 domain. *Cell* 130: 651–662
 29. Mari S, Ruetalo N, Maspero E, Stoffregen MC, Pasqualato S, Polo S, Wiesner S (2014) Structural and functional framework for the autoinhibition of Nedd4-family ubiquitin ligases. *Structure* 22: 1639–1649
 30. Escobedo A, Gomes T, Aragon E, Martin-Malpartida P, Ruiz L, Macias MJ (2014) Structural basis of the activation and degradation mechanisms of the E3 ubiquitin ligase Nedd4L. *Structure* 22: 1446–1457
 31. Wan L, Zou W, Gao D, Inuzuka H, Fukushima H, Berg AH, Drapp R, Shaik S, Hu D, Lester C et al (2011) Cdh1 regulates osteoblast function through an APC/C-independent modulation of Smurf1. *Mol Cell* 44: 721–733
 32. Wang J, Peng Q, Lin Q, Childress C, Carey D, Yang W (2010) Calcium activates Nedd4 E3 ubiquitin ligases by releasing the C2 domain-mediated auto-inhibition. *J Biol Chem* 285: 12279–12288
 33. Persaud A, Alberts P, Mari S, Tong J, Murchie R, Maspero E, Safi F, Moran MF, Polo S, Rotin D (2014) Tyrosine phosphorylation of NEDD4 activates its ubiquitin ligase activity. *Sci Signal* 7: ra95
 34. Bruce MC, Kanelis V, Fouladkou F, Debonneville A, Staub O, Rotin D (2008) Regulation of Nedd4-2 self-ubiquitination and stability by a PY motif located within its HECT-domain. *Biochem J* 415: 155–163
 35. Riling C, Kamadurai H, Kumar S, O'Leary CE, Wu KP, Manion EE, Ying M, Schulman BA, Oliver PM (2015) Itch WW domains inhibit its E3 ubiquitin ligase activity by blocking E2-E3 ligase trans-thiolation. *J Biol Chem* 290: 23875–23887
 36. Zhang W, Wu KP, Sartori MA, Kamadurai HB, Ordureau A, Jiang C, Mercredi PY, Murchie R, Hu J, Persaud A et al (2016) System-wide modulation of HECT E3 ligases with selective ubiquitin variant probes. *Mol Cell* 62: 121–136
 37. Gallagher E, Gao M, Liu YC, Karin M (2006) Activation of the E3 ubiquitin ligase Itch through a phosphorylation-induced conformational change. *Proc Natl Acad Sci USA* 103: 1717–1722
 38. Mund T, Pelham HR (2009) Control of the activity of WW-HECT domain E3 ubiquitin ligases by NDFIP proteins. *EMBO Rep* 10: 501–507
 39. Oliver PM, Cao X, Worthen GS, Shi P, Briones N, MacLeod M, White J, Kirby P, Kappler J, Marrack P et al (2006) Ndfip1 protein promotes the function of itch ubiquitin ligase to prevent T cell activation and T helper 2 cell-mediated inflammation. *Immunity* 25: 929–940
 40. Macias MJ, Hyvonen M, Baraldi E, Schultz J, Sudol M, Saraste M, Oschkinat H (1996) Structure of the WW domain of a kinase-associated protein complexed with a proline-rich peptide. *Nature* 382: 646–649
 41. Shi P, Xi Z, Wang H, Shi C, Xiong Y, Tian C (2010) Site-specific protein backbone and side-chain NMR chemical shift and relaxation analysis of human vinexin SH3 domain using a genetically encoded 15N/19F-labeled unnatural amino acid. *Biochem Biophys Res Commun* 402: 461–466
 42. Macias MJ, Wiesner S, Sudol M (2002) WW and SH3 domains, two different scaffolds to recognize proline-rich ligands. *FEBS Lett* 513: 30–37
 43. Kay BK, Williamson MP, Sudol M (2000) The importance of being proline: the interaction of proline-rich motifs in signaling proteins with their cognate domains. *FASEB J* 14: 231–241
 44. Aragon E, Goerner N, Xi Q, Gomes T, Gao S, Massague J, Macias MJ (2012) Structural basis for the versatile interactions of Smad7 with regulator WW domains in TGF- β pathways. *Structure* 20: 1726–1736
 45. Aki D, Zhang W, Liu YC (2015) The E3 ligase Itch in immune regulation and beyond. *Immunol Rev* 266: 6–26

46. Melino G, Gallagher E, Aqeilan RI, Knight R, Peschiaroli A, Rossi M, Scialpi F, Malatesta M, Zocchi L, Browne G et al (2008) Itch: a HECT-type E3 ligase regulating immunity, skin and cancer. *Cell Death Differ* 15: 1103–1112
47. Wood JD, Yuan J, Margolis RL, Colomer V, Duan K, Kushi J, Kaminsky Z, Kleiderlein JJ, Sharp AH, Ross CA (1998) Atrophin-1, the DRPLA gene product, interacts with two families of WW domain-containing proteins. *Mol Cell Neurosci* 11: 149–160
48. Solecki DJ (2012) Sticky situations: recent advances in control of cell adhesion during neuronal migration. *Curr Opin Neurobiol* 22: 791–798
49. Maspero E, Mari S, Valentini E, Musacchio A, Fish A, Pasqualato S, Polo S (2011) Structure of the HECT: ubiquitin complex and its role in ubiquitin chain elongation. *EMBO Rep* 12: 342–349
50. Chen Z, Jiang H, Xu W, Li X, Dempsey DR, Zhang X, Devreotes P, Wolberger C, Amzel LM, Gabelli SB et al (2017) A tunable brake for HECT ubiquitin ligases. *Mol Cell* 66: 345–357.e6
51. Jia M, Shan Z, Yang Y, Liu C, Li J, Luo ZG, Zhang M, Cai Y, Wen W, Wang W (2015) The structural basis of Miranda-mediated Staufien localization during *Drosophila* neuroblast asymmetric division. *Nat Commun* 6: 8381
52. Emsley P, Cowtan K (2004) Coot: model-building tools for molecular graphics. *Acta Crystallogr D Biol Crystallogr* 60: 2126–2132
53. Adams PD, Afonine PV, Bunkoczi G, Chen VB, Davis IW, Echols N, Headd JJ, Hung LW, Kapral GJ, Grosse-Kunstleve RW et al (2010) PHENIX: a comprehensive Python-based system for macromolecular structure solution. *Acta Crystallogr D Biol Crystallogr* 66: 213–221
54. Humphrey W, Dalke A, Schulten K (1996) VMD: visual molecular dynamics. *J Mol Graph* 14: 33–38, 27–28
55. Phillips JC, Braun R, Wang W, Gumbart J, Tajkhorshid E, Villa E, Chipot C, Skeel RD, Kale L, Schulten K (2005) Scalable molecular dynamics with NAMD. *J Comput Chem* 26: 1781–1802
56. MacKerell AD, Bashford D, Bellott M, Dunbrack RL, Evanseck JD, Field MJ, Fischer S, Gao J, Guo H, Ha S et al (1998) All-atom empirical potential for molecular modeling and dynamics studies of proteins. *J Phys Chem B* 102: 3586–3616
57. Shi P, Wang H, Xi Z, Shi C, Xiong Y, Tian C (2011) Site-specific (1)(9)F NMR chemical shift and side chain relaxation analysis of a membrane protein labeled with an unnatural amino acid. *Protein Sci* 20: 224–228
58. Xie Y, Juschke C, Esk C, Hirotsune S, Knoblich JA (2013) The phosphatase PP4c controls spindle orientation to maintain proliferative symmetric divisions in the developing neocortex. *Neuron* 79: 254–265